CRYSTALLIZATION KINETICS OF AMORPHOUS FERROMAGNESIAN SILICATE WITH OLIVINE-LIKE COMPOSITION. R. Sakurai[1], D. Yamamoto[2], A. Takigawa[1], and S. Tachibana[1] [1]Department of Earth and Planetary Science, University of Tokyo, Tokyo 113-0033, Japan (sakurai@eps.s.u-tokyo.ac.jp), [2]Department of Earth and Planetary Sciences, Kyushu University, Fukuoka 819-0395, Japan.

Introduction: Infrared spectroscopic observation of protoplanetary disks suggests that silicates, the major component of disk dust, occur in both amorphous and crystalline form [1, 2], with the crystalline fraction being higher in inner disks [3]. This indicates that amorphous silicate dust may crystallize in the warm inner disk.

The matrices of least altered/metamorphosed meteorites that are considered to preserve pristine dust in the protosolar disk show a predominance of amorphous silicates, mostly FeO-rich in composition [e.g., 4–6]. This means that such amorphous silicate dust avoided crystallization in the disk if they were originally present in the disk. It is therefore of importance to determine the crystallization kinetics of amorphous silicates to constrain the disk condition where amorphous silicate dust survives intact.

The solar abundance of Fe is comparable to that of Mg [7] and can be contained in amorphous silicate dust as FeO. While the crystallization kinetics of amorphous magnesium silicates have been determined [8, 9], the crystallization kinetics of FeO-bearing amorphous silicates have not been well determined because of the presence of hydroxides in the starting materials [10] and the assumption of pre-exponential factors [11, 12]. In this study, we performed crystallization experiments of amorphous ferromagnesian silicate particles with olivine-like composition and determined crystallization kinetics of the FeO-bearing amorphous silicate in vacuum.

Experiments: We used amorphous Mg-Fe silicate nanoparticles synthesized in an induction thermal plasma (ITP) system [13] at Nisshin Engineering Inc. as a starting material. The main component ("amorphous olivine" hereafter) was spherical particles with an average diameter of ~70 nm. The chemical composition was determined by using a field-emission electron probe microanalyzer (FE-EPMA; JEOL JXA-8530F) to be (Mg+Fe)/Si ratio of ~1.9 and Mg/(Mg+Fe) ratio of ~0.51. This composition is close to the solar abundance (Mg : Si : Fe ~ 1 : 1 : 1 [7]) . Si-rich amorphous silicate particles ((Mg+Fe)/Si ratio of ~0.8 and Mg/(Mg+Fe) ratio of ~0.54), probably produced by the previous ITP synthesis and left in the apparatus, were included as a contaminant.

Heating experiments were conducted at 580–630°C in vacuum (P_{H2O} ~10^{-4} Pa) for 0.5–162 hours. A sample of 30 mg was used in each experiment. Crystalline phases in the starting materials and run products were identified with X-ray diffraction (XRD; Rigaku RINT-2100) by using CuKα radiation (λ = 0.154178 nm) in the diffraction angle 2θ range from 10° to 90° with a step of 0.01° and a scan speed of 1° min^{-1}. The Mg/(Mg+Fe) ratio of olivine was determined from the position of the X-ray diffraction peak at 2θ of ~32° attributed to (130) spacing [14]. The 2θ values were calibrated using α-quartz powder as a standard sample. Infrared spectra of the starting materials and run products were obtained with a Fourier transform infrared spectrometer (FT-IR; JASCO FT/IR-4200). After the experiments, each sample was mixed into KBr powder with a mass ratio of 1 : 500, and 200.4 mg of the mixed powder was pressed into a thin pellet. Infrared spectra of the samples were obtained with a spectral resolution of 2 cm^{-1}.

Results and Discussion: The starting material contained a small amount of crystalline olivine (Fo_{52}) and metallic iron. The disappearance of XRD peaks attributed to metallic iron in all heated samples indicates the metallic iron was incorporated into the amorphous olivine during heating up to the experimental temperature. The XRD patterns of all heated samples showed that only olivine crystals were crystallized. The olivine composition ranged within $Fo_{52–65}$ during progress of crystallization, and reached to $Fo_{\sim57}$ (580°C), $Fo_{\sim55}$ (610°C), and $Fo_{\sim52}$ (630°C) at the end of crystallization. Although the crystallized olivine had a slightly higher Mg/(Mg+Fe) ratio than the amorphous olivine, no FeO-free olivine (forsterite) crystallized throughout the entire crystallization process. By contrast, amorphous olivine originally has a slightly lower (Mg+Fe)/Si ratio than the olivine stoichiometry ((Mg+Fe)/Si = 2), so the amorphous residue is expected to become enriched in SiO_2 as the olivine crystallizes.

The degree of crystallization x_{cr} was quantitatively estimated by fitting the infrared absorption spectra of the heated samples at wavelengths ranging from 8 μm to 13 μm as a combination of the starting material (defined as $x_{cr} = 0$) and the longest heated sample at each temperature (defined as $x_{cr} = 1$) (Figure 1). The temporal evolution of crystallization degree of amorphous olivine was fitted with the Johnson-Mehl-Avrami (JMA) equation [15, 16] only for points with $x_{cr} < \sim0.7$ to eliminate possible deceleration of crystallization due to SiO_2 enrichment in the amorphous phase with

crystallization of olivine. The Si-rich contaminant in the starting material has no effect on this fitting since we confirmed in preliminary experiments that it does not crystallize at all during the experimental time.

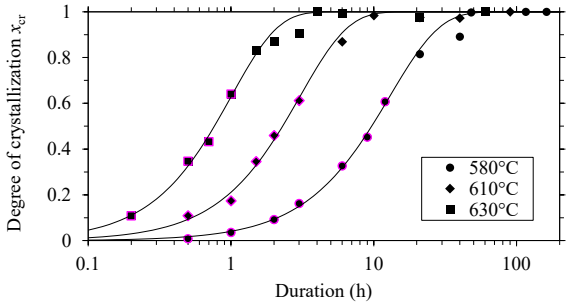

Figure 1. Temporal evolution of crystallization degree of amorphous olivine. For each temperature, fitted curves with the JMA equation for points with degree of crystallization x_{cr} below ~0.7 are also shown.

The obtained Avrami constant n of 1.2–1.3 in this study is close to 1.5, which is suggestive of three-dimensional diffusion-controlled growth from the pre-existing crystalline nuclei as in the case of crystallization of amorphous forsterite in vacuum [8]. The Arrhenius relation of the reciprocal of the crystallization timescale τ (timescale required for x_{cr} ~ 0.63) gives the activation energy for amorphous olivine crystallization of 323.9 ± 9.4 kJ mol^{-1} and the pre-exponential factor ln ν_0 (s^{-1}) of 34.9 ± 1.6 (Figure 2). The low activation energy compared with that for crystallization of amorphous silicate with forsterite composition (414.4 ± 7.0 kJ mol^{-1} [8]) suggests that the presence of FeO in the amorphous structure may promote the structural changes necessary for olivine crystallization, specifically the breakage of Si-O-Si bonds and/or the diffusion of network-forming elements (i.e., Si and O).

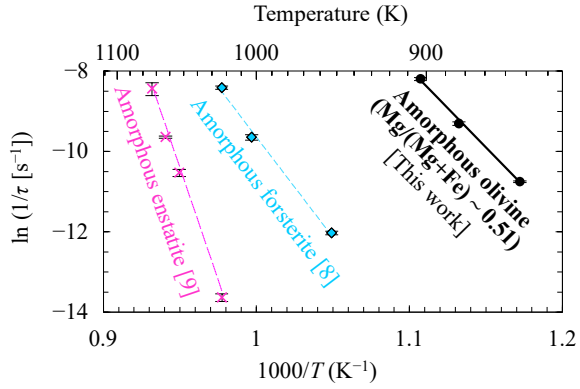

Figure 2. Arrhenius plots of the reciprocal of the crystallization timescale τ for crystallization of amorphous olivine in this study and of amorphous silicates with forsterite and enstatite compositions [8, 9].

The present study suggests that crystallization of amorphous olivine always proceeds at least 3–4 orders of magnitude faster than for FeO-free amorphous silicates [8, 9] (Figure 3). The temperature required for amorphous silicate dust with an olivine-like composition (Fe/Mg ~ 1) to avoid crystallization in the disk is ~100 K lower than that for amorphous forsterite (Fe/Mg = 0). This implies that crystalline forsterite particles and FeO-bearing amorphous silicate in the matrices of least metamorphosed carbonaceous chondrites have different origins although it is critically important to understand the origin of FeO-bearing amorphous silicates.

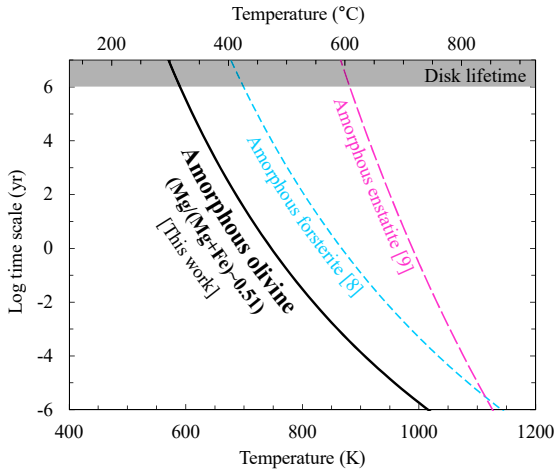

Figure 3. Crystallization timescale τ of amorphous olivine, and of amorphous silicate with forsterite and enstatite compositions [8, 9] as a function of annealing temperatures.

References: [1] Henning T. (2010) *Annu. Rev. A&A, 48,* 21–46. [2] Sargent B. A. et al. (2009) *ApJS, 182,* 477–508. [3] van Boekel R. et al. (2004) *Nature, 432,* 479–482. [4] Brearley A. (1993) *GCA, 57,* 1521–1550. [5] Scott E. R. D. and Krot A. N. (2005) *ApJ, 623,* 571–578. [6] Abreu N. M. and Brearley A. J. (2010) *GCA, 74,* 1146–1171. [7] Lodders K. (2003) *ApJ, 591,* 1220–1247. [8] Yamamoto D. and Tachibana S. (2018) *ACS Earth Space Chem., 2,* 778–786. [9] Murata K. et al. (2009) *ApJ, 697,* 836–842. [10] Murata K. et al. (2007) *ApJ, 668,* 285–293. [11] Brucato J. R. et al. (2002) *P&SS, 50,* 829–837. [12] Djouadi Z. et al. (2005) *A&A, 440,* 179–184. [13] Sakurai R. et al. (2020) *LPS LI,* Abstract #2844. [14] Brown G. E. (1982) In *Orthosilicates,* 275–381. [15] Johnson W. A. and Mehl R. F. (1939) *Trans. Am. Inst. Min. Engin., 135,* 416–442. [16] Avrami M. (1939) *J. Chem. Phys., 7,* 1103–1112.